PMAS
Proceedings of the Mongolian Academy of Sciences
Vol. 64 No 02(250) 2024
DOI: https://doi.org/10.5564/pmas.v64i02.3648

ARTICLE

Magnetospheric response on impact of solar wind diamagnetic structures borne by eruptive prominence

***Parkhomov Vladimir Alexandrovich*[1*], *Eselevich Victor Grigorieivich*[2], *Tsegmed Battuulai*[3] *and Eselevich Maksim Victorovich*[2]**

[1]*Department of Mathematical Methods and Digital Technologies, Baikal State University, Irkutsk, Russian Federation*
[2]*Department of Solar Physics, Institute of Solar-Terrestrial Physics, Siberian Branch (ISTP SB), Russian Academy of Sciences, Irkutsk, Russian Federation*
[3] *Department of Geomagnetism, Institute of Astronomy and Geophysics, Mongolian Academy of Sciences, Ulaanbaatar, Mongolia*

ARTICLE INFO: Received: 06 Dec, 2023; Accepted: 04 June, 2024

Abstract: We address the sequence of Sun-to-Earth phenomena, that enables to study the mechanism for geoefficiency of eruptive prominences propagating from the Sun inside coronal mass ejections (CMEs). An eruptive prominence ejected in the solar wind (SW) moves at the SW velocity Earthward like a diamagnetic structure of eruptive prominence (DSEP).The key feature of the latter is a largesharp plasma concentration jump *N* inside the DSEP at a simultaneous sharp drop in the interplanetary magnetic field (IMF) modulus B. It is the anti-correlation between the *N* and *B* profiles in DSEP, due to which its contact with the magnetosphere may lead not only to magnetosphere compression, but also to penetration of DSEP substance into the magnetosphere. The duration of the magnetospheric disturbance (in the form of dayside auroras), global increase in the current systems, charged particle flux enhancement in the radiation belts, and generation of the irregular Pi2-3 oscillations are determined by the DSEP size. We present statistical investigations into DSEPs observed in different years of solar activity and built a qualitative model for DSEP geoefficiency.

Keywords: *eruptive prominence, diamagnetic structure of eruptive prominence, saw-tooth substorm, double auroral oval, Pi2-3 geomagnetic pulsations;*

INTRODUCTION

In [22], there was a notion of slow solar wind (SW) diamagnetic structure (DS) geoefficiency. Those structures are detected by the negative correlation coefficient between great jumps in the SW concentration and in the interplanetary magnetic field (IMF) modulus. They are transported away from the Sun to the Earth orbit by slow SW fluxes.

Most major geomagnetic disturbances are related to sporadic SW. Its sources on the Sun are coronal mass ejections (CMEs). In the Earth orbit, a sporadic SW is recorded like a sequence comprising a shock, a sheath (the compression region ahead of a CME), and an interplanetary coronal mass ejection (ICME).

***Corresponding author, email**: pekines_41@mail.ru* *https://orcid.org/0000-0004-0637-8979*

to [6], it may appear either like a magnetic cloud (MC), or like an ejecta. It is inside the MC and the ejecta, where an eruptive prominence (EP) is

Vol. 64 No 02(250) 2024
DOI: https://doi.org/10.5564/pmas.v64i02.3648

recorded. The latter features a sharp and a big jump in the plasma concentration N with a simultaneous sharp decrease in the IMF modulus. Withthis feature, it is an explicit DS of sporadic SW [23]. Further, we refer to this structure as a diamagnetic structure of eruptive prominence (DSEP), thus emphasizing its source.

By now, the Sun prominence has been established to represent a magnetic rope with plasma colder than the solar corona plasma surrounding it. Two bases of this rope are anchored to the photosphere. In the Hα line, on the solar limb, the rope is usually observed like a higher-brightness arch loop, and like a lower-brightness filament on the disk. Under certain conditions, there may occur an eruption of prominence and its propagation towards the Earth. This process often (but not always) accompanies the formation of a sporadic SW source that a CME is. In some rare cases, a prominence eruption is regarded as a reason for a CME generation [9,10]. However, this issue has not been studied comprehensively.

The purpose of this study is to conduct a detailed investigation into the nature and the character of magnetosphere disturbance capable of causing EP-related DSs.

MATERIALS AND METHODS

We investigated the variations in the SW-flux plasma concentration N and in the IMF modulus B inside DSs and DSEPs from measurements at the liberation points in the orbits of the ACE and the WIND, near the Earth with the Geotail, IMP-8, and INTERBALL-1, as well as with the POLAR located inside the magnetosphere. Fig. 1 shows the position of the satellites.

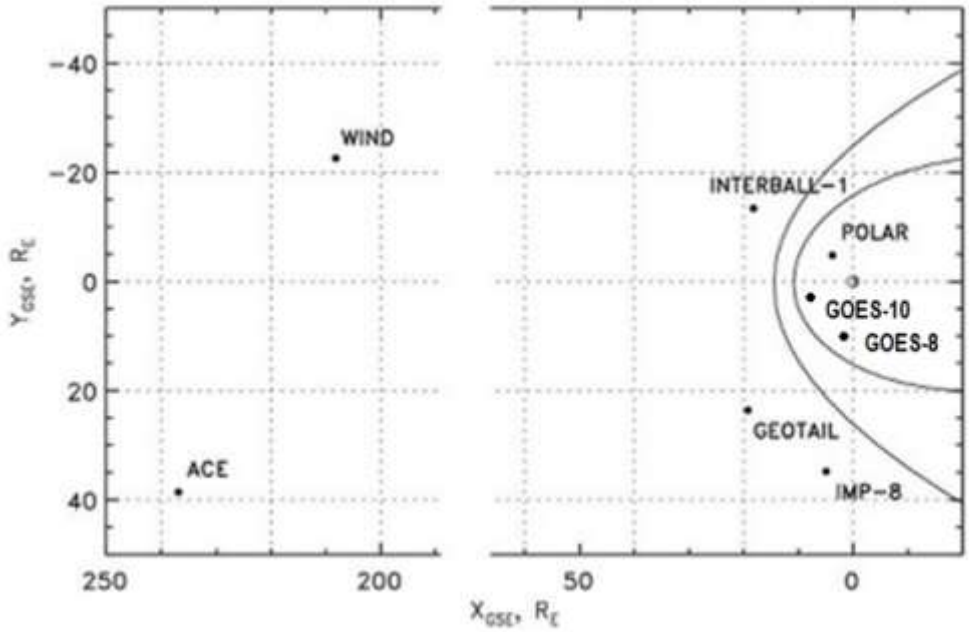

Figure 1. 1999 Jul 2 positions of the satellites inside and outside the magnetosphere

We also used the data from ground-based geomagnetic observations at the INTERMAGNET global network, from the Circum-pan Pacific Magnetometer Network (CPMN, 210 magnetic meridian) [30], from the CARISMA network, as well as observational data from induction magnetometers at the Borok (BOX) and

Vol. 64 No 02(250) 2024
DOI: https://doi.org/10.5564/pmas.v64i02.3648

Mondy (MND) observatories. Table 1 provides the names and the coordinates of the observatories.

Table 1. Names and coordinates of observatories

No	Station name and abbreviation	Geographic latitude, deg.	Geographic longitude, deg.
1	Alibag (ABG)	18.62	72.87
2	Barrow (BAR)	71.32	203.38
3	Borok (BOR)	58.03	38.33
4	Chokurdakh (CHD)	70.62	147.89
5	Dawson (DAW)	64.05	220.89
6	Guam (GUA)	13.59	144.87
7	Honolulu (HON)	21.02	201.94
8	Kakioka (KAK)	36.23	263.96
9	Kanoya (KNY)	31.42	130.88
10	Kotel'nyy (KTN)	75.94	137.71
11	Kouror (KOU)	5.21	307.27
12	Lermonth (LMT)	–22.22	114.1
13	Mondy (MND)	52.10	104.42
14	Magadan (MGD)	59.97	150.86
15	Mquarie Isl. (MCQ)	–54.50	158.95
16	Mboor (MBO)	14.28	343.03
17	Paratunka (PET)	52.94	158.25
18	Pamatai (PPT)	-17.57	210.42
19	Resolute Bay (RES)	74.69	265.10
20	Sun Juan (SJG)	18.07	293.5
21	Tixi (TIX)	71.53	128.78
22	Thule (THL)	77.47	290.77
23	Tamanrasset (TAM)	22.79	5.53

Detection and analysis of 1999 Jul 2 dsep in Earth Orbit

Before detecting the EP source on the Sun and analyzing the results of DSEP recording with different spacecraft, we remind the characteristic EP properties inside a solar corona CME in the ecliptic plane. They are listed in [1,2, 24].

1. An eruptive prominence represents a loop with inhomogeneous boundaries and is located inside a CME magnetic cavity that corresponds to an MC at 1 AU.

2. The filament loop thickness ΔL_p, along the radius R (towards the X axis of the CME motion), is much smaller than the similar size ΔL_{CME} for CME.

3. The filament loop thickness towards Z, perpendicular to the ecliptic plane, is comparable with the ΔL_p.

4. The angular size of the CME and of the eruptive filament roughly persists while moving to the Earth orbit.

Figure 2 shows the results of comparing the observations of the eruptive filament at its motion from the libration orbit to ~$4R_E$.

PMAS
Proceedings of the Mongolian Academy of Sciences
Vol. 64 No 02(250) 2024
DOI: https://doi.org/10.5564/pmas.v64i02.3648

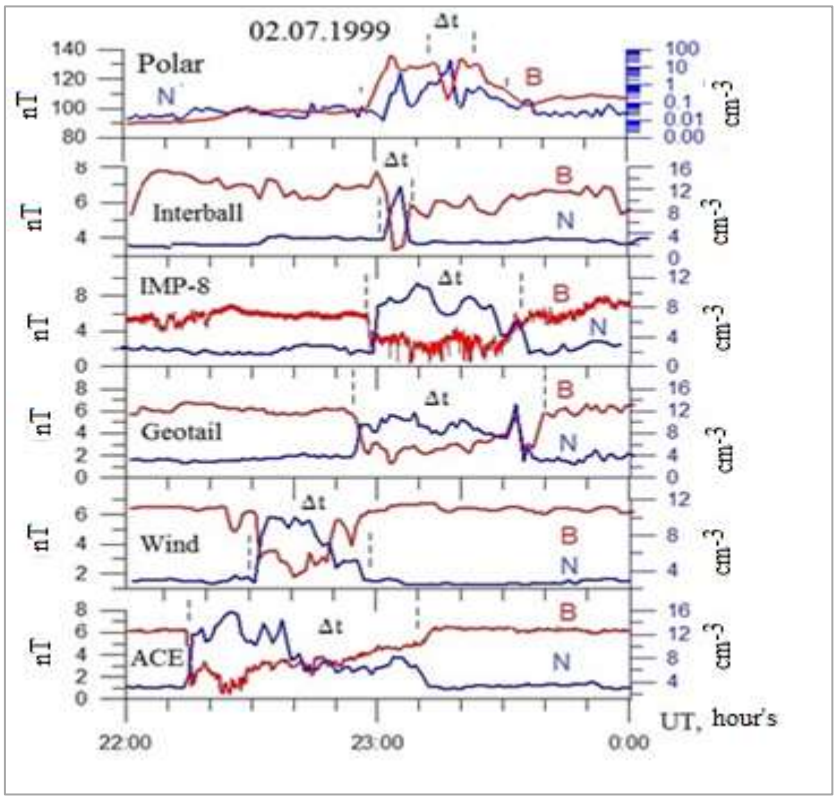

Figure 2. Variations in the plasma concentration N (blue curves) and in the IMF modulus B (red curves) in the 1999 Jul 2 DSEP region, recorded at different spacecrafts. Bottom-to-top: ACE, WIND, GEOTAIL, IMP-8, INTERBALL-1, POLAR; Δt is the time interval, when the filament passed through the satellite (vertical dashed lines show its two-time boundaries)

The vertical dashed lines in Fig. 2 mark the instants, when a spacecraft crossed the front and the back filament boundaries, Δt is the time interval, during which the filament passed through a satellite. Apparently, both boundaries (by recording the time) are significantly shorter than the duration Δt (filament passing through a satellite). Here with, one observes an anti-correlation between the N and B variations at all the satellites in SW and at the Polar inside the magnetosphere on the dayside at ~$4R_E$. It is this fact that allows us to interpret (for the first time) the EP (filament) in the solar wind as a DSEP, and to show the penetration of this structure into the magnetosphere.

At different spacecrafts, the time intervals Δt significantly differ (see Fig. 2). Because the velocity for all the sites is nearly identical (and equals about V_{SW}~630 km/s), let us estimate the spatial size ΔL_p towards the X axis, recorded with different spacecrafts. For the ACE, $\Delta L_{pACE} = \Delta t_{ACE} V_{CB.}$ Similarly, we determined the spatial size of the filament from measurements at another spacecraft.

As a result, we obtained (in R_E): $\Delta L_{p\,WIND} \approx 178R_E$; $\Delta L_{p\,ACE} \approx 356R_E$; $\Delta L_{pGeotail} \approx 237R_E$; $\Delta L_{p\,Interball\text{-}1} \approx 30R_E$.

In Fig. 2 (top panel), one can see that the N and B profile anti-correlation persists inside the magnetosphere up to ~$4R_E$, and is recorded by the Polar. Hence, there comes an important conclusion of the DSEP penetration into the magnetosphere.

Let us estimate its spatial size ΔL_{pPolar}. For that purpose, we determined the average radial velocity V_{In} for the DSEP motion between the Interball-1 and the

PMAS
Proceedings of the Mongolian Academy of Sciences
Vol. 64 No 02(250) 2024
DOI: https://doi.org/10.5564/pmas.v64i02.3648

Polar. The distance on the X axis between them is $\Delta x \approx (17.5 - 4.8)\ R_E \approx 12.7 R_E$. The UT time interval between them $\Delta t \approx$ (23:02:30 - 22:58:00) ≈ 270 s. Then, $V_{In\ P} \approx$ 300 km/s, $\Delta L_{pPolar} \approx 104.5 R_E$.

In Fig. 3, black dots show a strong inhomogeneity of the cross-section size $\Delta Lp/Re$ along the Y axisin the ecliptic plane. The dagger marks the Polar-recorded $\Delta Lp/Re$ inside the magnetosphere.

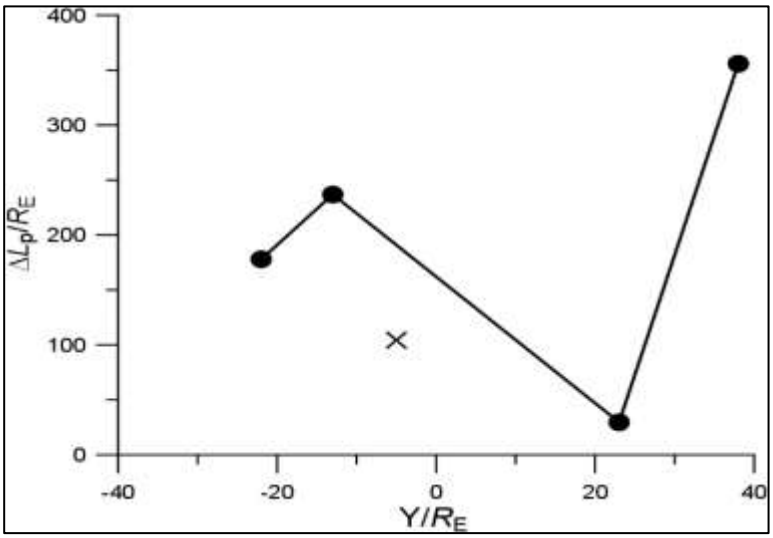

Figure 3. DSEP ΔL_pdependence on the distance along the Y axis(normalization to R_E) in the ecliptic plane. The dagger marks the Polar-recorded$\Delta L_p/R_E$ inside the magnetosphere

Apparently, the cross-section size $\Delta L_p/R_E$ of the DSEP extended along the Y-axis (i.e., towards the X axis) may vary more than tenfold already at $y \leq 10 R_E$.

This conclusion completely agrees with those in [24], where the authors similarly analyzed the 1999 Jul 2 event for the first time, but without considering the fact that the object is a DS capable of penetrating into the magnetosphere.

Detecting the source of the 1999 Jul 2 eruptive prominence recorded in the Earth Orbit

Let us address the source of the 1999 Jul 2 DSEP recorded in the Earth orbit at about 22:00-24:00 UT (Fig.4a). This site is a part of a sporadic SW flux that comprises a sequence of structures: a shock recorded at ~01:00 UT, impact warmed plasma, and an MC. The selection of this DSEP site located inside the magnetic cloud is related to that it is this site that enables to study (most scrupulously and sequentially) a typical coupling between a DESP and the magnetosphere.

First of all, let us detect the sporadic SW source on the Sun (Fig. 5). A preliminary analysis for some CMEs [https://cdaw.gsfc.nasa.gov/CME_list/] showed that the nearest most probable source of the addressed sporadic SW may be a halo CME that was accompanied by the N18E07 X-ray M3.3 flare. The 1999 Jun 29 flare onset time is $t_0 \approx$07:31 UT (Fig. 4).

PMAS
Proceedings of the Mongolian Academy of Sciences
Vol. 64 No 02(250) 2024
DOI: https://doi.org/10.5564/pmas.v64i02.3648

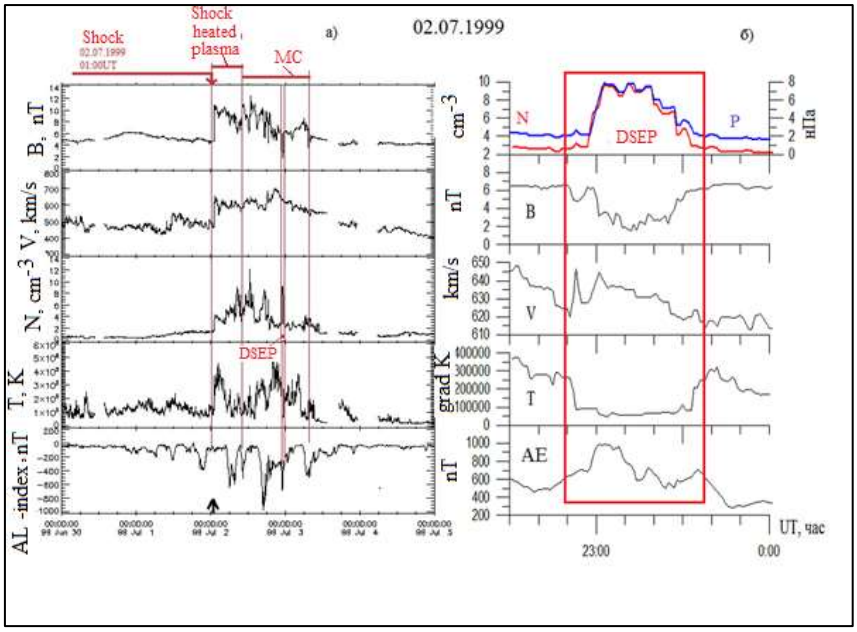

Figure 4a - Variations in the parameters of the 1999 Jun 30 - Jul 5 sporadic ejecta-type SW involving a DSEP. Top-to-bottom: B is the IMF modulus, V is the SW velocity, N is the SW proton concentration, T is the SW temperature, AL is the index of auroral magnetic activity; b - DSEP parameters at the 1-min resolution. Top-to-bottom: N is the SW proton concentration, P is the SW kinetic pressure, B is the IMF modulus, V is the SW velocity, T is the SW temperature, AE is the index of auroral magnetic activity. Note a sharp temperature drop, equal in duration to the DSEP recording time, and a sharp short-time burst of auroral magnetic activity

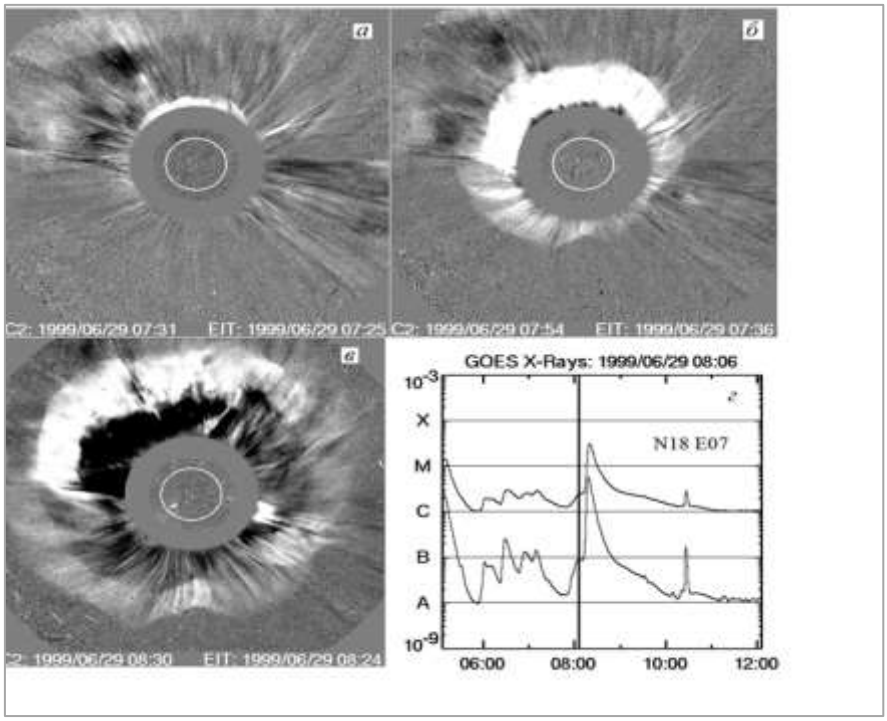

Figure 5. Sequence of white corona difference images from the C2 LASCO coronagraph (a-c). Inside the white circle (corresponding to the Sun surface), there are different images in the 193 Å channel; X-rays profiles (d) from the GOES within the 1.0-8.0 Å (upper curve) and 0.5-4.0 Å ranges [https://cdaw.gsfc.nasa.gov/CME_list/catalog_description.htm]

PMAS
Proceedings of the Mongolian Academy of Sciences
Vol. 64 No 02(250) 2024
DOI: https://doi.org/10.5564/pmas.v64i02.3648

Let us estimate a possibility that this halo CME (1999 Jun 29, 07:31 UT) might be a source for the 1999 Jul 2 DSEP. Fig. 5 (*a-d*) shows its time evolution like a sequence of white corona difference images from the C2 LASCO.

As per to catalog [https://cdaw.gsfc.nasa.gov/CME_list/], in the limb plane its average initial velocity is $V_{0\ \mathrm{limb}} \approx 634$ km/s. In the radial direction along the Sun-to-Earth line, the average initial velocity of this CME site, according to [27] $V_{0\ \mathrm{S\text{-}E}} \approx 1.8 V_{0\ \mathrm{limb}} \approx 1141$km/s. Knowing the CME initial velocity toward the Earth $V_{0\,\mathrm{S-E}}$, we may estimate the arrival time of this CME site in the Earth orbit, as well as its velocity in the Earth orbit. The average velocity of this halo CME $V_{\mathrm{av\ S\text{-}E}}$ between the Sun and the Earth, according to [7],

$$V_{\mathrm{av\ S\text{-}E}} \approx 3/4\ V_{0\,\mathrm{S\text{-}E}}, \quad (1)$$

and its velocity $V_{\mathrm{e\ S\text{-}E}}$ at 1 AE.

$$V_{\mathrm{e\ S\text{-}E}} \approx V_{0\,\mathrm{S\text{-}E}}/2 \quad (2)$$

By formulas (1) and (2), we find $V_{\mathrm{av\ S\text{-}E}} \approx 856$ km/s, $V_{\mathrm{e\ S\text{-}E}} \approx 570$ km/s. Let us estimate the time ΔT for the Sun-to-Earth motions of this CME site: $\Delta T \approx 215 R\mathrm{sun}/V_{\mathrm{av\ S\text{-}E}} \approx 1.5 \cdot 10^8$ [km]/856 [km/s] ≈175234 with ≈ 48.67 h ≈ 2 days 0.67 h.

The emergence time of the addressed CME on the Sunas of 1999 Jun 29 is $t_0 \approx 07{:}31$ UT; its arrival time at 1 AE $t_e \approx t_0 + \Delta T \approx 00{:}40$ UT on 1999 Jul 02 (vertical arrow in Fig. 4). Herewith, the calculated SW velocity at 1 AE $V_{\mathrm{e\ S\text{-}E}} \approx 570$ km/s differs insignificantly from the recorded velocity ~630 km/s. Thus, the Sun source of the addressed DSEP is the halo CME emerged on 1999 Jun 29 at $t_0 \approx 07{:}31$ UT.

Magnetospheric response

The DSEP in the Earth orbit was recorded at 22:47 UT, according to OMNI [https://cdaweb.gsfc.nasa.gov/cdaweb/istp_public/](Fig. 4b). To determine the structure lifetime and to define the time of its coupling with the magnetosphere, we used the Wind observational data on the SW concentration and the IMF modulus at the 3-s resolution.

One can see that the *N* and *B* main jump at 22:57 UT was preceded by two smaller-intensity jumps. Therefore, we accept the onset of the DSEP contact with the magnetosphere at a 13-min shift relative to the *N* and *B* main jump timeat 22:57 UT. We address the response features in two frequency ranges: the low-frequency in the current systems determined by ring current variations (*SYM-H* indices of geomagnetic activity), auroral current jet variations (*SML* and *SMU* indices), and the high-frequency determined by the dynamics of the Pi 2-3 irregular geomagnetic pulsations (T = 180 ÷ 320 s).

Response in magnetospheric current systems

Fig. 6*a* shows the DSEP *N*, *B*, *By*, *Bz* parameters from OMNI, the magnetospheric response in the geomagnetic field variations at low-latitude magnetic observatories, in the *SML, SMU,* and *SYM-H* geomagnetic activity indices. We can split the magnetospheric response into four stages. Stages 1-2 correspond to the coupling onset caused by a sharp temperature drop and a slight increase in the kinetic pressure (Fig. 4b); stages 2-3 correspond to the DCF phase, a sharp enhancement of currents at the magnetopause, caused by the

Vol. 64 No 02(250) 2024
DOI: https://doi.org/10.5564/pmas.v64i02.3648

magnetosphere compression through an SW jump from 2.8 to 10 cm^{-3} and through the kinetic pressure jump from 4.1 to 8 nP. The kinetic pressure jump is predominantly related to a sharp concentration increase, because the SW velocity within this interval changes insignificantly (628 ±10 km/s). The value for the magnetopause current caused by a pressure jump may be determined through the formula $b \times P^{-0.5}$ from the model in [21], here P is the SW kinetic pressure, while the coefficient b = 7.26 was obtained in [12]. The *SYM-H* jump value computed by the above formula equaled 22.7 nT, which is close to the value presented at the CDWEB [3].

The IMF B_x and B_y components in the ecliptic plane reverse their direction spasmodically at the DCF onset, while the B_z smoothly changes its direction from south to north. Probably, in the addressed event, the IMF components in the horizontal plane appeared geoeffective together with the pressure jump.

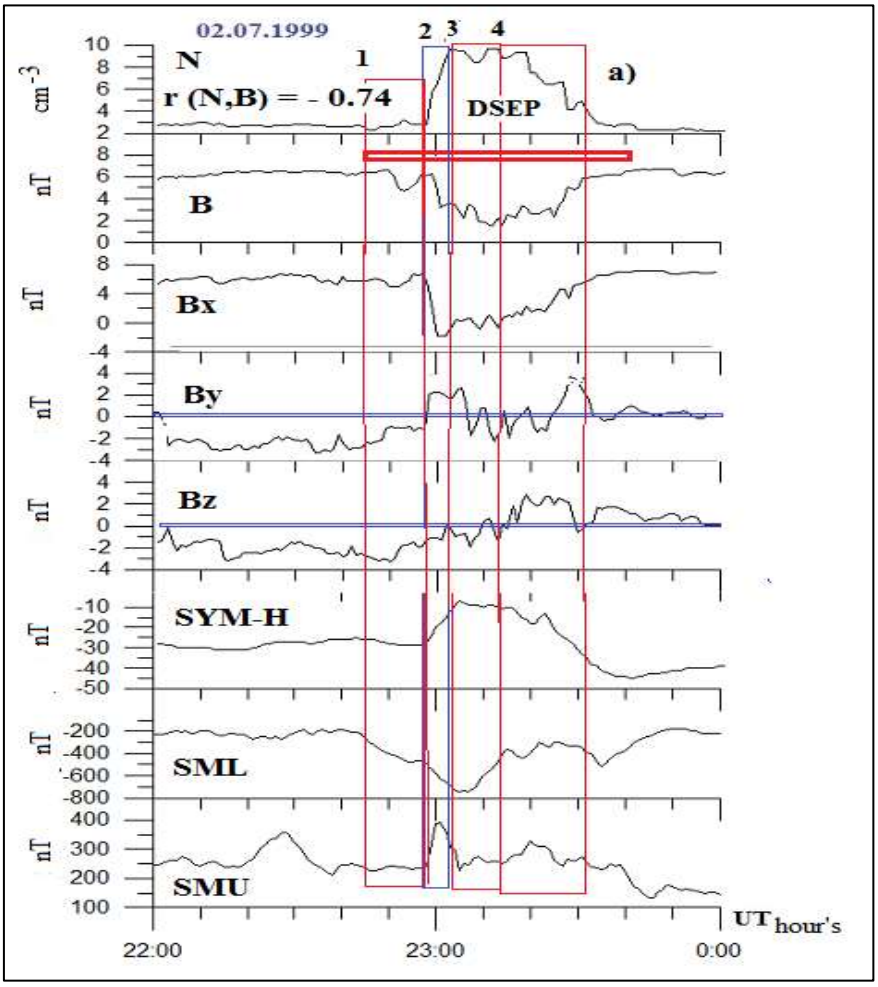

Figure 6a. Global magnetospheric response to the 1999 Jul 2 DSEP arrival at the Earth: a (top to bottom) - SW concentration N and IMF modulus B from 3-min Wind observations, ring current index SYM-H, western auroral electrojet index SML, east current index SMU. 1 - onset of contact with DSEP, 2 - onset of DSEP coupling with the magnetopause (DCF phase onset), 3 - DCF phase end at low-latitude observatories and the DR (ring current) value stabilization, 4 - Pi2-3 oscillation generation

PMAS
Proceedings of the Mongolian Academy of Sciences
Vol. 64 No 02(250) 2024
DOI: https://doi.org/10.5564/pmas.v64i02.3648

Stages 3-4 imply a DR increase caused by the magnetosphere compression and by a sharp jump of the IMF *By* component. Stage 4 represents generating a train of damped Pi 2-3 oscillations induced by the power transformation of the DSEP that penetrated into the magnetosheath and affected the magnetopause. Fig. 6*b* more explicitly shows the details of the effect from the stages.

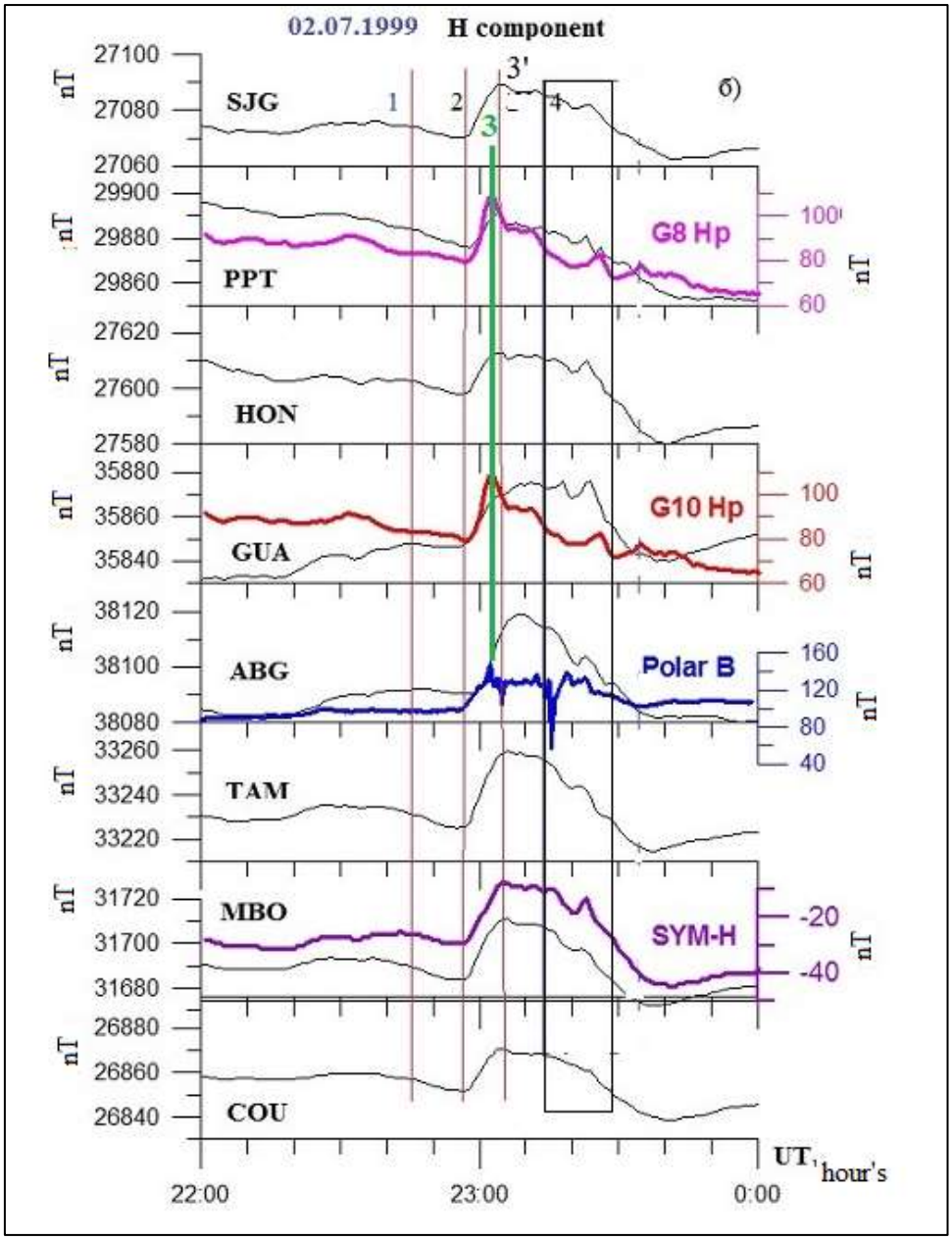

Figure 6b. Fragments of magnetograms from low-latitude observatories, depending on local time. 1 - onset of contact with DSEP, 2 - onset of the DSEP coupling with the magnetopause (DCF phase onset), 3 - DCF phase end at satellites, 3' - DCF phase end at low-latitude observatories and the DR value stabilization, 4 - generation of Pi2-3 oscillations. The following elements have been added (as compared with Fig. 6a): SYM-H at the dawn observatory and the data from the Polar satellites (modulus B), GOES-10, GOES-8 (H_p-components), depending on their position in local time [https://cdaweb.gsfc.nasa.gov/cdaweb/istp_public/]

Vol. 64 No 02(250) 2024
DOI: https://doi.org/10.5564/pmas.v64i02.3648

All the satellites, whose data are provided in Fig. 6b, were on the dayside: Polar - ~9 h, GOES-10 - ~13 h, GOES-8 - ~17 h MLT. GOES-10 recorded an H_p-componentsharp jump by ~ 50 nT; GOES-8 on the dusk side recorded a jump by 40 nT. The geomagnetic field modulus at the Polar in the pre-midday sector spasmodically increased by ~60 nT. The east auroral electrojet index *SMU* increases spasmodically from ~250 to 400 nT. The geomagnetic field increases (by duration) are almost equal to the time, when the DSEP front edge was passing through the satellites.

On the Earth, the planetary magnetic activity dramatically increased at ~22:47 UT. The DSEP contact with the magnetosphere caused a sharp global magnetic activity growth determined by a synchronous increase in the auroral magnetic activity indices (*SML* by ~600 nT and *SMU* by 250 nT) and by a ring current increase (*SYM-H* grew by ~20 nT). These DSEP forcing effects on the magnetosphere may be realized by using the mechanism addressed in [12, 18].

The essence of the mechanism is that the geomagnetic storm evolution is governed by both the interplanetary magnetic field and the solar wind kinetic pressure. They generate the necessary conditions for plasma entry into the inner magnetosphere. In our case, the ring current increase occurs at the storm recovery phase, but not at the initial phase of its evolution, like in the quoted paper.

One can also obtain the information on energy entry into the magnetosphere from the analysis of variations in the charged particle (electrons) fluxes and in the magnetic field modulus at the Polar (Fig. 7a). Over the indicated short interval, *Ne* and *B* vary opposite in phase. By proving the anti-correlation and by considering a large difference in the sampling frequency of the measured parameters, we provide the fragments of the files that record these parameters in the figure. The extreme *Ne* and *B* values were recorded at about the same time: 23.16:29 and 23.16:20 UT respectively. We specifically point out to the absolute anti-correlation between the charged particle concentration and the geomagnetic field modulus. The module of geomagnetic field decreased dramatically to ~57 nT, which is considerably lower than the dipole geomagnetic field value at L ~ 4. Simultaneously, with the jump in *Ne* and *B*, there is a sharp increase in the spectral power of the precipitating ion flux in between 0.275 eV and 320 keV (Fig. 7b). This enables to conclude that the Polar recorded a diamagnetic structure that penetrated deeply into magnetosphere (up to 4 Re). This implies that a portion of the DSEP energy permeates not only into magnetosheath, but also inside the magnetosphere. We can see this in Fig. 7*a* and *b* (rectangle 1), which corresponds to the stage 4 maximum in Fig. 6*a* and *b*.

This result agrees with the data obtained earlier by [23] and by other authors [13, 16]. Those data indicate a pulse entry of the SW energy into the magnetosphere. Theoretical and model calculations also corroborate this result [19, 5].

PMAS
Proceedings of the Mongolian Academy of Sciences
Vol. 64 No 02(250) 2024
DOI: https://doi.org/10.5564/pmas.v64i02.3648

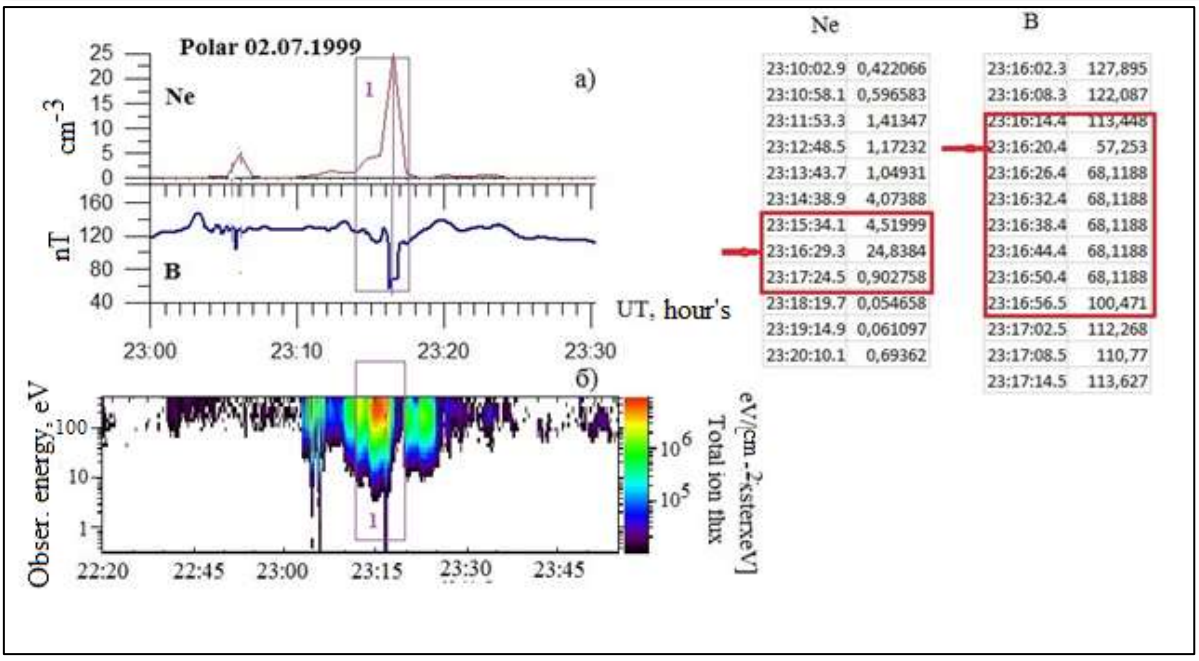

Figure 7a - electron flux Ne and the geomagnetic field modulus B at the Polar in the magnetosphere dawn sector; b– The file fragments are within the red rectangles. The arrows indicate the instants with the most (least) parameter values. b -Spectrogram for the ion flux at the Polar. Rectangle 1 marks the interval corresponding to the DSEP part entry into the magnetosphere. Ne, B and a fragment of files obtained from spacecraft measurements of values

Response in irregular PI 2-3 pulsation dynamics (T = 180÷320 s)

In [23,13], the authors revealed the generation of irregular Pi2-3 geomagnetic pulsations at the SW DS energy pulse passage into the magnetosphere. First of all, we note that the effect of dramatic inhomogeneities (interplanetary shocks, pressure jumps, and disruptions) on the magnetosphere leads to the generation of bursts of broadband ULF Psc 1-6 pulsations within 1÷600 s [20].

Let us now address the features of the geomagnetic pulsation mode at the DSEP contact with the magnetosphere. Fig. 8*a-d* presents the geomagnetic pulsation spectrograms and magnetogram fragments at the high-latitude Dauson (DAW) observatory that was near the midday meridian (MLT = UT - 10.3) during recording. In the *H*-component 23:13 through 23:30 UT within 160-240, one can clearly see an oscillation train (blue rectangle) with the maximal amplitude of ~200 nT. The average period of the maximal oscillation intensity on the spectrogram equals ~ 170 s, which is higher than the Pi2 period in the International Classification of Irregular Pulsations (40-150 s) [11]. Therefore, this period corresponds to the Pi3 range [20]. At the same time, at the low-latitude BOR, MND, KAK (Fig. 8*d*), the oscillation spectral density maximum occupies the same range of periods (150-220 s) that is close to the Pi2 range. Therefore, considering the bandwidth of periods, we will further refer to such a train as Pi2-3 pulsations. For the addressed event (Fig. 8*a-c*), the frequency period does not depend on the observation point longitude, which points to a common oscillation source. Such a source may be MHD waves generated at dramatic magnetic field variations owing to the passage of plasma clots (jets) through the magnetosheath plasma. Such waves (with a 140-s delay) were observed inside the magnetosphere [13].

PMAS
Proceedings of the Mongolian Academy of Sciences
Vol. 64 No 02(250) 2024
DOI: https://doi.org/10.5564/pmas.v64i02.3648

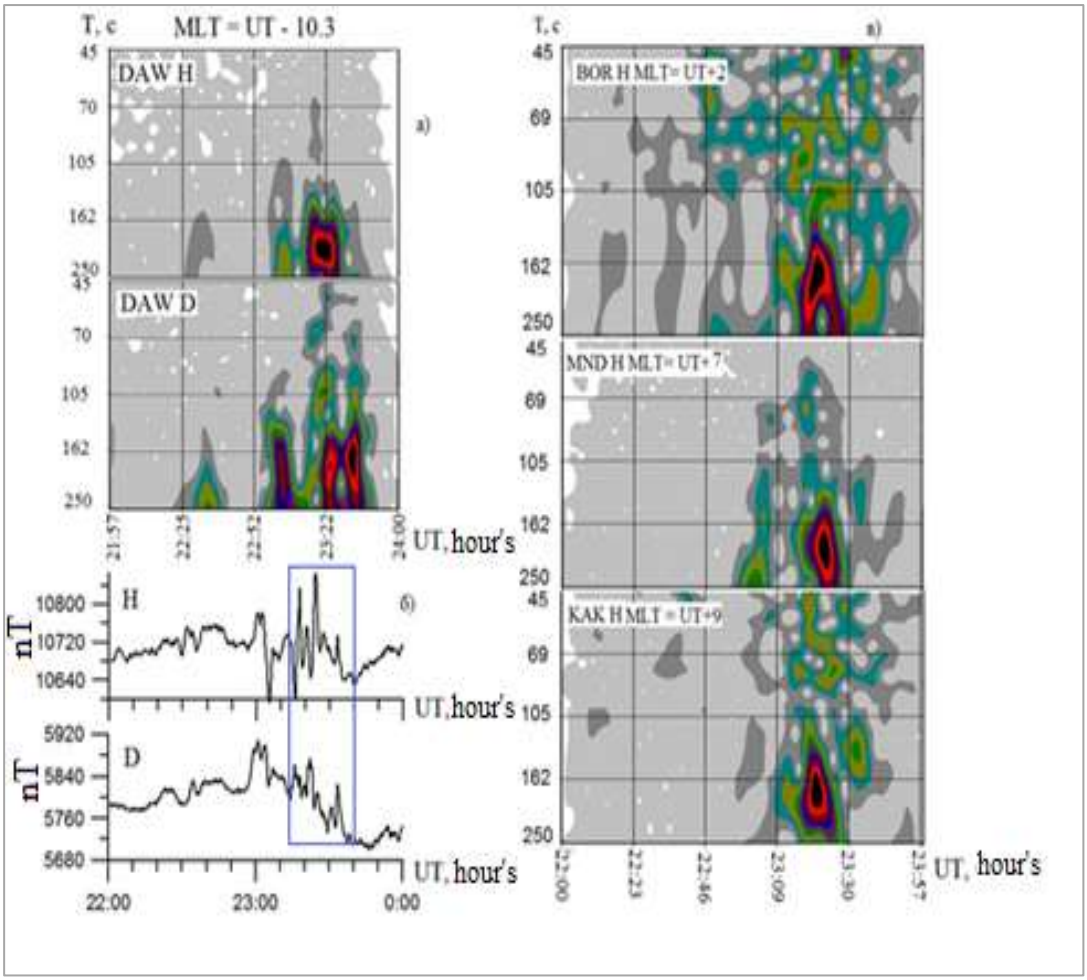

Figure 8. Geomagnetic pulsation spectrograms (a), fragments of magnetograms from the midday DAW observatory within the CARISMA network (b), and geomagnetic pulsation spectrograms from the BOR, MND, and KAK observatories in the midnight-dawn sector (c)

One can clearly see the global nature of the magnetospheric response to the contact with DSEP and the globality of generating a geomagnetic pulsation train on the magnetograms from the meridional chain observatories from the auroral region to the equator (210 magnetic meridian) including for the Macquarie Island (MCQ) conjugate observatory in the Southern Hemisphere [30] (Fig. 9 a,b). The local time of the meridional stations was 9:00 MLT. For comparison, we also provide the midday Barrow observatory data. For all the observatories, particularly for the mid-latitude ones, one can see a simultaneous bay disturbance with a superposition of the Pi2-Pi3 pulsation train.

PMAS
Proceedings of the Mongolian Academy of Sciences
Vol. 64 No 02(250) 2024
DOI: https://doi.org/10.5564/pmas.v64i02.3648

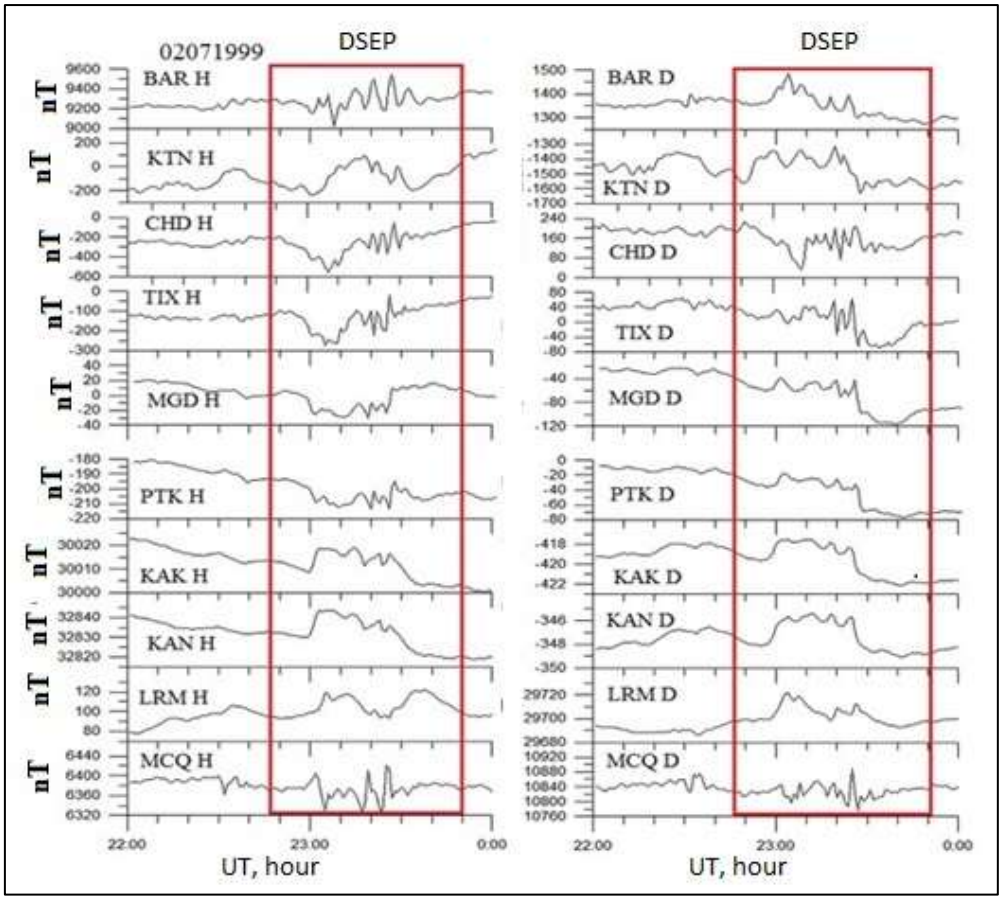

Figure 9. Fragments of magnetograms for the H- and D-components from the CPMN observatories (210° MM) [http://denji.02geo.kyushu-u.ac.jp/]. Red rectangle shows the DSEP observation time. Blue rectangle presents the interval of recording the Pi 2-3 train

Auroral response to contact with DSEP

Fig.10*a* shows the sequence of evolution in auroras reflecting the DSEP coupling with the magnetosphere and recorded by the UVI instrument onboard the Polar [28]. On the first frame (22:19:49 UT), there is no auroral activity detected. On the following frame (22:29:21 UT) in the 08-05 LT dawn sector at ~63° N, there emerges a quiet arch extended along the parallel. At 22:38:23 UT, there emerges a transpolar strip of auroras (a surge across the polar cap), that exists until 22:52:47 UT. At 22:58:28 UT, one can see an activity increase from the dusk side. On the 22:38:23 UT frame, the glow intensifies in the dusk and midnight sectors. At 23:03:39 UT, the glow encompasses the entire oval of auroras within ~62°-74°, and the second auroral oval emerges at ~70°. Such a shape of auroras is peculiar to saw-tooth substorms. The maximal auroral intensity is observed 23:09:30 UT through 23:20:33 UT. On the 23.20.33 UT frame, one can see a displacement of the glow region northward. Then, the auroral activity damps, and auroras cease after ~23:50 UT, when the SW *N* and the DSEP *B* return to the undisturbed level.

Analyzing the observations of the auroras emerging after the DSEP contact with the magnetosphere shows a cardinal difference in the evolution of auroral shapes from the dynamics of the auroras accompanying (on the magnetosphere

Vol. 64 No 02(250) 2024
DOI: https://doi.org/10.5564/pmas.v64i02.3648

midnight side) the substorm, whose cause is magnetosphere tail processes. In a classic substorm, one observes a regular sequence of phenomena. At the initial stage, in the near-midnight Harang discontinuity, there emerges an initial brightening, the intensity of which dramatically turns into the explosion phase, and the auroral bend moves westward [14]. In the addressed event, the atmospheric glow starts on the dayside, moving west- and eastward from midday. We addressed a similar auroral dynamics earlier for the 1999 Jun 28 event [25]. The auroral dynamics also differ from "shock auroras" [31] that start on the dayside after the magnetosphere contact with interplanetary shocks, and the glow propagates eastward at ~6-11 km/s. Note the features of the atmospheric glow on the frames from 22:41:54 UT to 23:31:35 UT (Fig. 10*a*), where one can see the emergence of the second glow strip northward from the main strip of the auroral oval. For clarity, panel *b* presents an enhanced frame with the atmosphere glow details in the UVI range at 23:18:38 UT. Arrows 1 and 2 designate the first and the second strips. We emphasize that one observes such an auroral shape during saw-tooth substorms [29]. Another feature peculiar to saw-tooth substorms is the injection of high-energy particles in a geostationary orbit.

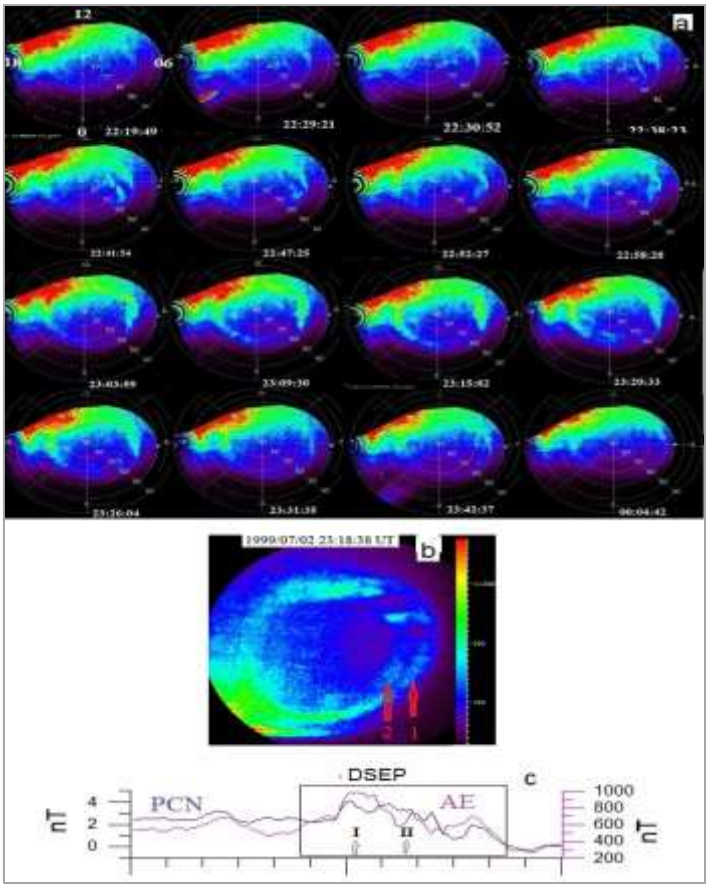

Figure 10a - Sequence of auroral shots (Polar, UVI instrument). The frames reflect the DSEP coupling with the magnetosphere, and auroral evolution from the dayside. One can see the emergence of the second oval there on frames 23:09:30 UT through 23:31:35 UT; b - enhanced frame, arrows 1 and 2 indicate the auroral ovals; c - variations in the PCN and AE indices. Arrow 1 indicates the onset of the second auroral strip emergence, arrow 2 shows the shot time

Vol. 64 No 02(250) 2024
DOI: https://doi.org/10.5564/pmas.v64i02.3648

According to the description for the saw-tooth substorm evolution dynamics [29], one observes a strict correspondence between the magnetic activity variations in the polar cap and the evolution of magnetic disturbances in the auroral region. In the case of DSEP coupling with the magnetosphere, one can also see such a coupling that manifests itself through a sync between the variations in the AE index determining the ionospheric current strength in the auroral region and the *PCN* index determining the ionospheric current strength in the polar cap. The correlation coefficients between *PCN-AE*, *PCN-AL* equal 0.78 and -0.65, respectively.

Thus, as a result of the DSEP coupling with the magnetosphere, we observe the following phenomena:

1. A global response in the ionospheric currents of the polar cap, of the auroral region, and of the ring current.

2. Aurora intensification. It starts on the midday side and the glow extends to the dusk and dawn sides. When the activity is at its maximum, there emerge patterns like a double auroral oval.

3. Dramatic intensification of electron and ion fluxes in the Polar orbit inside the magnetosphere. The fluxes are opposite in phase to the geomagnetic field modulus variations. This is similar to the proton concentration variations being opposite in phase to the SW DSEP IMP modulus.

4. Variations in the polar cap ionospheric currents. They are synchronous with the auroral region ionospheric current variations ($r_{AE,\,\mathrm{PCN}} = 0.78$).

5. Generation of the Pi2-Pi3 global train. The above phenomena are peculiar to a substorm, but have a number of features that do not allow us to relate them to a classical substorm. The latter is generated due to an explosive release of the SW energy stored through the mechanism for the power line reconnection in the geomagnetic field and in the IMP at the magnetosphere tail. We note that features 1-6 are more peculiar to a saw-tooth substorm. This allows us to assume that the observed response to the DSEP coupling with the magnetosphere may be classified as an elementary act (one tooth) of a saw-tooth substorm.

This idea is not new. In [4], based on investigating 213 isolated substorms and 184 separate saw-tooth events through a magnetogram inversion technique, the authors drew a conclusion that the signatures of saw-tooth event DP-1 current system potential is similar to the signatures of isolated substorms. But a saw-tooth event DP-1 potential cell covers a larger area and shows a greater variability than similar cells of the isolated substorm: the saw-tooth substorm potential average trend increases by 70 kV 30 min after the substorm onset, whereas it grows by only 35 kV for isolated substorms. The authors, by comparing the characteristics for two types of substorms, found that saw-tooth events may be more diverse. The authors arrived at the conclusion that in terms of ionospheric electrodynamics, saw-tooth events have features similar to those of isolated substorms. although they are larger by spatial extent and by value.

This evidences that there may be several mechanisms causing individual teeth in a saw-tooth substorm. In [26], the authors investigated (through a superposed epoch analysis) 155 isolated substorms, 122 periods of steady magnetospheric convection, and 138 cases of saw-tooth substorms. They draw the conclusion that the SW velocity is the key parameter determining magnetospheric and ionospheric activity.

Vol. 64 No 02(250) 2024
DOI: https://doi.org/10.5564/pmas.v64i02.3648

Both above investigations are based on large statistics, and their conclusions emphasize problems of specifying SW/IMF solar sources and parameters determining magnetospheric activity. The main conclusion in both the papers is that magnetospheric disturbances are determined by the processes of SW energy accumulation in the magnetosphere tail and its subsequent release in a substorm.

Unlike the above and many other papers, we found that DSEP coupling with the magnetosphere causes a geomagnetic disturbance like a moderate substorm, whose evolution (unlike the classic case) starts on the midday side of the magnetosphere. Its onset is initiated by the magnetosphere contact with the DSEP, when the IMF vertical component changes its direction from south to north. Besides, we note the fact that the magnetospheric disturbance duration coincides the time of the DSEP coupling with the magnetosphere. In other words, the energy dissipates in the magnetosphere as it enters. We detected similar phenomena for other events as well [23, 25].

RESULTS

Statistical results

As statistical data, we provide a table for DSEP observations for different years of solar activity. The data were selected arbitrarily for different years in the solar cycle of total 151 cases, when the WIND observed ICMEs [https://wind.nasa.gov/ICMEindex.php].

No	Date	Onset UT	Duration min	D*SYMH* nT	D*AL* nT	D*N* cm^{-3}	D*B* nT	V_{mean} km/s	B_z, nT – before + after	$r_{B,N}$	$r_{AE,\ PCN}$	$r_{AL,\ PCN}$	Flare importance
1	1998 Jun 26	9:55	30	40	150	17	4	476	0	–0.92	0.41	–0.36	[22]
2	1999 Jun 28	4:50	60	50	150	28	4	900	0/+4	–0.8	0.75	–0.41	M2.3 [4]
3	1999 Jul 2	21:20	40	20	500	10	4	600	–2/+12	–0.92	0.78	–0.65	M3.3[24]
4	2000 Jun 11	17:30	80	26	800	28	6	590	–10/8(–5)	–0.9	0.53	–0.45	No data
5	2001 Apr 4	18:00	60	–28	440	4	4	780	10/–12+12	–0.88	0.78	–0.73	X10 [15]
6	2001 Apr 13	9:50	80	62	2300	12	8	800	–5/+5	–0.72	0.94	–0.92	M 2.3
7	2001 Oct 21	20:25	60	50	1000	50	6	635	–20/0(-20)	–0.7	0.43	–0.6	No data
8	2005 Jan 21	18:40	70	60	500	40	14	940	-24/+30	–0.8	0.6	–0.66	X8 [17]
9	2007 May 22	13:00	160	20	200	14	5	435	–4/+8	–0.76	0.87	–0.81	M1
10	2011 Jun 5	0:00	190	20	1000	10	5	530	0/+10	–0.54	0.38	–0.86	C5
11	2011 Aug 5	19:50	55	60	1200	30	26	620	–20/+10	–0.84	0.31	–0.2	M10
12	2014 Jun 8	6:00	30	21	1000	5	5	550	–14/+20	–0.7	0.83	–0.8	M2.5
13	2014 Sep 8	4:35	45	18	100	12	4	450	–11/+5	–0.69	0.92	–0.67	M1
	Mean values		73.85	32.23	718,46.	20.00	7.31	638.92		–0.78	0.66	–0.62	
	RMS deviation		48.10	25.11	608,84.	14.09	6.25	166.47		0.11	0.22	0.21	

Vol. 64 No 02(250) 2024
DOI: https://doi.org/10.5564/pmas.v64i02.3648

In the table, we highlighted (in bold) the events, whose investigation results are published and presented in the references.

The parameters in the table allow us to draw the following conclusions.

1. The average time of the DSEP existence is ~74 min; at the average SW velocity ~ 639 km/s, the average pattern size is ~$2.8 \cdot 10^6$ km.

2. The geomagnetic response manifests itself predominantly in the *SYM-H* positive growth by 32 nT and in a sharp auroral activity increase (AL) by ~720 nT.

3. The geomagnetic response onset coincides with a sharp change in the direction of the IMF vertical component from south to north.

4. The average correlation coefficient between the SW concentration and the IMF modulus is ~0.78.

5. High values of the correlation coefficients between *AE -PCN and AL -PCN* confirm synchronism of ionospheric current variations in the auroral region and the polar cap.

6. If one considers the sample representative, one can see that the DSEP generation (ejection) does not depend on the flare X-ray importance.

Principal results

1. The cross section of the eruptive prominence as a part of a magnetic cloud in the Earth orbit is shown to feature dramatic jumps in plasma concentration N and opposite-in-phase high-correlated (R ~-0.8) jumps in the IMF modulus B. At the boundaries of jumps, there is a sharp change in the azimuth angle Φ and in the IMF vector latitude angle Θ. Also sharp temperature drop occurs at the boundaries of jumps. This allows us to draw the conclusion that eruptive prominences are diamagnetic patterns.

2. The filament effect on the magnetosphere is one reason for activating magnetospheric processes, whose duration is determined by the cross-sectional size of the filament, i.e., by the time of the filament effect on the magnetosphere. Magnetospheric disturbances start on the magnetosphere dayside like auroras in the midday sector and extend to the dawn and dusk sides of the magnetosphere.

There occurs global generation of irregular Pi2-Pi3 pulsations with a ~170-250 s period the onset (start; commencement) in the observatory arranged (localized; located) near midday meridian.

All this evidences that there is an evolution of a high-latitude magneto-ionospheric disturbance different from a classic substorm type.

3. The obtained results meet the ideas in [29], according to which magnetic saw-tooth-disturbances start against the background of high auroral activity with a typical pattern of the double auroral oval. For such disturbances, one observes a strict correspondence between the magnetic activity variations in the polar cap and the ionospheric current intensity variations in the auroral region.

4. The obtained result agrees with the conclusions in [4] that, in terms of the ionospheric electrodynamics, saw-tooth events have the features similar to those of isolated substorms.

CONCLUSIONS

In conclusion, we present a general qualitative model for DSEP propagation (Fig. 11 *a-d*). The structure originates as a result of a prominence/filament eruption at

Vol. 64 No 02(250) 2024
DOI: https://doi.org/10.5564/pmas.v64i02.3648

a CME emergence near the Sun surface, and then propagates as a CME part to the Earth orbit and beyond. The filament (DSEP) effect on the magnetosphere leads to the compression of the latter and, simultaneously, to penetration of the DSEP energy portion into the magnetosphere. The DSEP energy is spent on particle acceleration in the radiation belts, electron precipitation into the atmosphere, and generation of auroras, as well as for the ionospheric ionization growth, ring current and auroral electrojet increases, and generation of the Pi2-Pi3 pulsations with amplitudes comparable to those of a substorm bay disturbance.

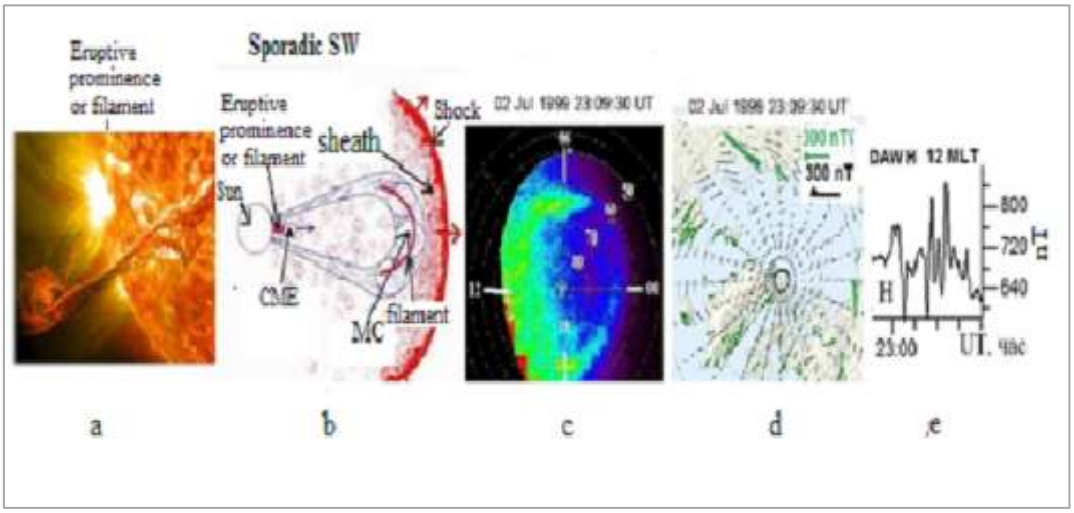

Figure 11. Qualitative model for the SW DSEP structure Sun-to-Earth propagation: a - example for a prominence (filament) eruption on the Sun; b- characteristic parts of a sporadic SW flux; c - auroral response to the DSEP contact; d - vector diagram of the ionospheric currents [8]; e - magnetogram fragment presenting a Pi2-Pi3 record at the observatory at near-midday hours

Acknowledgements

The authors express their sincere gratitude to the NASA CDAWEB team for providing the ACE, Wind, Geotail, IMP-8, Polar, GOES-8, GOES-10 data.

We are thankful to the colleagues at the Institute of Space Research of the Russian Academy of Sciences for using the Interball-1 data. We are grateful to I.R. Mann, D.K. Milling and other members of the CARISMA team allowing us to use their data. We thank K. Yumoto and the CPMN group for the 210 MM data. We acknowledge the contribution of Dr. Jesper W. Gjerloev by providing us with the SUPERMAG data. We are indebted to S.V. Anisimov, Director of the BOROK Geophysical Observatory at the Schmidt Institute of Physics of the Earth of the Russian Academy of Sciences, for providing us with the data from induction magnetometers. The results were obtained by using the Angara Multi-Access Center facilities (http://ckp-rf.ru/ckp/3056/). The study was done within the 2022-2023 State Budget Research Issue of the Baikal State University "System Analysis and Information Processing Methods in Space Research." The contribution of V.G. Eselevich and M.V. Eselevich was supported by a financial support from the Ministry of Education and Science of the Russian Federation (Minobrnauki of Russia).

Vol. 64 No 02(250) 2024
DOI: https://doi.org/10.5564/pmas.v64i02.3648

REFERENCES

1. Burlaga L. Microscale structure in the interplanetary medium. Solar Phys. 1968. No. 4. pp. 67-98. https://doi.org/10.1007/BF00146999
2. Burlaga L., Sitteler E, Mariani F., Schwenn R. Magnetic loop behind an interplanetary shock: Voyager, Helios and IMP-8 observations. J. Geophys. Res. 1981. V. 86, no. 8. pp. 6673-6684, https://doi.org/10.1029/JA086iA08p06673
3. Burton R. K., Mcpherron R. L., Russel C. T. An empirical relationship between interplanetary conditions and Dst. J. Geophys. Res. 1975, V. 80, No 31, pp. 4204 – 4214, https://doi.org/10.1029/JA080i031p04204
4. Cai X., Clauer C. R., Ridley A. J. Statistical analysis of ionospheric potential patterns for isolatedsubstorms and sawtooth events. Ann. Geophys., 2006, V. 24, pp. 1977-1991, https://doi.org/10.5194/angeo-24-1977-2006
5. Echim M. M., Lemaire J. F. Laboratory and numerical simulations of the impulsive penetration mechanism. Space Sci. Rev., 2000, V. 92. pp. 565-601, https://doi.org/10.1023/A:1005264212972
6. Ermolaev Yu. I., Nikolaeva N. S., Lodkina I. G., and Ermolaev M. Yu. Catalog of large-scale phenomena in the solar wind over 1976-2000 Kosmicheskiye Issledovaniya (Space Research). 2009. V. 47, No. 2. pp. 99-113., in Russian.
7. Eselevich M. V, and Eselevich V. G.. Sporadic plasma flows and their sources during extreme solar activity 2003 October 26 through 2003 November 6. Kosmicheskiye Issledovaniya (Space Research). 2004. V. 42, No. 6. pp. 595-607, in Russian.
8. Gjerloev J. W. The SuperMAG data processing technique. J. Geophys. Res. 2012, vol. 117, iss. A9, A09213. https://doi.org/10.1029/2012JA017683
9. Grechnev V. V., Lesovoi S. V., Kochanov A. A., et al. Multi-instrument view on solar eruptive events observed with the Siberian Radioheliograph: From detection of small jets up to development of a shock wave and CME. J. Atmos. and Solar-Terr. Phys. 2018. V 174. pp. 46-65. https://doi.org/10.1016/j.jastp.2018.04.014
10. Grechnev V. V., Uralov A. M., Kochanov A. A., et al. A tiny eruptive filament as a flux-rope progenitor and driver of a large-scale CME and wave. Solar Phys. 2016. V. 291. pp. 1173-1208. https://doi.org/10.1007/s11207-016-0888-z
11. Guglielmi A. V., and V. A. Troitskaya. Geomagnitnyye pul'satsii i dignostika magnitosfery (Geomagnetic pulsations and magnetosphere diagnostics). Moscow, Nauka Publishers, 1973. P. 208., in Russian.
12. Kalegaev V. V., Vlasova N. A., and Peng Zh.. Magnetosphere dynamics during geomagnetic storms. Kosmicheskiye Issledovaniya (Space Research). 2015, V. 53, No. 2. pp. 105-117., in Russian.
13. Katsavriasi C., Rapits S., Daglis L. A. Karlsson T., Georgiou N., Balasis G. On the generation of Pi2 pulsations due to plasma flow patterns around magnetosheath jets. Geophys. Res. Lett.

Vol. 64 No 02(250) 2024
DOI: https://doi.org/10.5564/pmas.v64i02.3648

2021. V. 48, e2021GL093611. https://doi.org/10.1029/2021GL093611

14. Kepko L., McPherron R. L., Amm O., Apatenkov S., Baumjohann W., Birn J., Lester M., Nakamura R., Pulkkinen T. I., Sergeev V. Substorm current wedge revisited. Space Sci. Rev. 2015. V. 190, pp. 1-46. https://doi.org/10.1007/s11214-014-0124-9
15. Kim K. H., Catell C. A., Lee D. H., Takahashi K., et.al. Magnetospheric responsesto suddem and quasiperiodic solar wind variations. J. Geophys. Res.2002, V. 107, No. A11,1406; https://doi.org/10.1029/2002JA009342
16. Klibanova Yu. Yu., Mishin V. V, Tsegmed B. and Moiseev A. V. Properties of daytime long-period pulsations during magnetospheric storm commencement. Geomagnetism and Aeronomy. 2016, V. 56, No. 4, pp. 426-440, https://doi.org/10.1134/S0016793216040071
17. Kozyra J. U., Liemohn M. W., Cattell C. et al. Solar filament impact on 21 January 2005: Geospace consequences. J. Geophys. Res. Space Physics, V. 119, pp. 5401-5448, https://doi.org/10.1002/2013JA019748
18. Mishiin V. V., Klibanova Y. Y.,Medvedev A. V., Mikhalev, A. V., Penskikh , Y. V., Marchuk R. A. Bursts geomagnetic pulsations and night atmosphere airglow caused by solar wind pressure changes during magnetosphere storm. Doklady Earth Sci. V. 504(1), pp. 390-394, https//doi.org/10.1134/S1028334X22060125
19. Lemaire J. Plasmoid motion across a tangential discontinuity (with application to the magnetopause). J. Plasma Phys. 1985. Vol. 33, No. 3. pp. 425-436, https://doi.org/10.1017/S0022377800002592
20. Nishida A. Geomagnitnyy Diagnoz Magnitosfery (Geomagnetic Diagnosis of the Magnetosphere). Moscow: Mir Publishers, 1980. P. 300, in Russian
21. O'Brien, McPherron R. L., An empirical phase space analysis of ring current dynamics: Solar wind control of injection and decay J. Geophys. Res. 2000, V. 105, No. A4, pp. 7707 – 7719, https://doi.org/10.1029/1998JA000437
22. Parkhomov V. A, Eselevich V. G., Eselevich M. V., Dmitriev A. V., and Vedernikova T. I.. Diamagnetic plasmoids as components of the "slow" solar wind diamagnetic structures, and their effect on the Earth magnetosphere. Solnechno-Zemnaya Fizika (Solar-terrestrial physics). 2019. V. 5. No. 4, pp. 42-54. https://doi.org/10.12737/szf-54201905
23. Parkhomov V. A, Eselevich V. G., Eselevich M. V., Dmitriev A. V., Suvorova A. V., Khomutov S.Yu., Tsegmed B., and Tero Raita. Magnetospheric response to a coupling with a diamagnetic structure of the sporadic solar wind. Solnechno-Zemnaya Fizika (Solar-terrestrial physics). 2021. V. 7, No. 3. pp. 12-30. https://doi.org/10.12737/szf-73202102
24. Parkhomov V. A, Borodkova N. L., Eselevich V. G., Eselevich M. V., and Zastenker G. N.. Dramatic changes in the plasma concentration within the sporadic solar wind and their effect on the Earth magnetosphere. Kosmicheskiye Issledovaniya (Space Research). 2015. V. 53, No. 5. pp. 1-12.

Vol. 64 No 02(250) 2024
DOI: https://doi.org/10.5564/pmas.v64i02.3648

DOI: 10.7868/S002342061505009X, in Russian.

25. Parkhomov V. A, Borodkova N. L., Eselevich V. G., Eselevich M. V., Dmitriev A.V. , and Chilikin V .E.. Features of the impact of the solar wind diamagnetic structure on Earth's magnetosphere. Solar-Terrestrial Physics. 2017. Vol. 3, No. 4, pp. 44–57. https://doi.org/10.12737/szf-34201705
26. Partamies N., Pulkkinen T. I., McPherron R. L., McWilliams K., Bryant C. R., Tanskanen E., Singer H.J ., Reeves G. D., Thomsen M. F. Statistical survey on sawtooth events, SMCs and isolated substorms. Adv. Space Res. 2009. V. 44, No 4, pp. 376-384. https://doi.org/10.1016/j.asr.2009.03.013
27. Schwenn R., Dal Lago A., Huttunen E., Gonzalez W. D. The association of coronal mass ejections with their effects near the Earth. Ann. Geophys. 2005. V. 23. No 3, pp. 1033-1059. https://doi.org/10.5194/angeo-23-1033-2005
28. Torr M. R., Torr D. G., Zukic M., Johnson R. B., J. Ajello, Banks P., et al. A far ultraviolet imager for the International Solar-Terrestrial Physics Mission. Space Sci. Rev. 1995. V. 71. pp. 329-383, https://doi.org/10.1007/BF00751335
29. Troshichev O., Stauning P., Liou K., Reeves G. Saw-tooth substorms: inconsistency of repetitive bay-like magnetic disturbances with behavior of aurora. Adv. Space Res. 2011. V. 47. Iss. 4, pp. 702-709. https://doi.org/10.1016/j.asr.2010.09.026
30. Yumoto K. and the MAGDAS Group. MAGDAS project and its application for space weather ILWS WORKSHOP - 2006. GOA, February 19-24, 2006. pp. 1-7.
31. Zhou X. Y., Tsurutani B. T. Rapid intensification and propagation of the dayside aurora: Large-scale interplanetary pressure pulses (fast shocks). Geophys. Res. Lett. 1999. V. 26, iss. 8. pp. 1097-1100. https://doi.org/10.1029/1999GL900173 .